



HAL
open science

Contribution à l'étude de l'écoulement du fluide et du transfert de chaleur dans des bains de fusion au cours du soudage à l'arc TIG

Koffi Koudadje, Clarisse Delalondre, Marc Medale, Jean-Michel Carpreau

► To cite this version:

Koffi Koudadje, Clarisse Delalondre, Marc Medale, Jean-Michel Carpreau. Contribution à l'étude de l'écoulement du fluide et du transfert de chaleur dans des bains de fusion au cours du soudage à l'arc TIG. CFM 2013 - 21ème Congrès Français de Mécanique, Aug 2013, Bordeaux, France. <hal-03441122>

HAL Id: hal-03441122

<https://hal.science/hal-03441122v1>

Submitted on 22 Nov 2021

HAL is a multi-disciplinary open access archive for the deposit and dissemination of scientific research documents, whether they are published or not. The documents may come from teaching and research institutions in France or abroad, or from public or private research centers.

L'archive ouverte pluridisciplinaire **HAL**, est destinée au dépôt et à la diffusion de documents scientifiques de niveau recherche, publiés ou non, émanant des établissements d'enseignement et de recherche français ou étrangers, des laboratoires publics ou privés.



HAL Authorization

A numerical and experimental study of heat and mass transfer during GTA welding of different austenitic stainless steels

K. KOUDADJE^a, M. MEDALE^b, C. DELALONDRE^a, J. M. CARPREAU^c

a. EDF Research & Development, CHATOUE (France)

b. Aix-Marseille University IUSTI CNRS UMR 7343, MARSEILLE (France)

c. LaMSID, UMR EDF-CNRS-CEA 2832, CLAMART (France)

Résumé : *Les caractéristiques d'un cordon de soudage à l'arc TIG dépendent fortement des mouvements de convection dans le bain de fusion au cours de l'opération. Un modèle numérique de transferts thermiques et d'écoulement dans le bain de fusion a été développé et implémenté dans Code_Saturne® (code open source de calcul en mécanique des fluides développé par EDF R&D) pour étudier la soudabilité des aciers inoxydables. Les principales forces prises en compte dans ce modèle sont la force de tension de surface (Marangoni), les forces électromagnétiques et la gravité. Par ailleurs, des essais de soudage ont été réalisés avec différents paramètres de soudage sur des éprouvettes d'aciers 304L de différentes concentrations en soufre afin de valider les résultats numériques obtenus.*

Abstract : *During GTA welding, properties of resulting weld are significantly affected by the weld pool convection. In this study, a numerical model has been developed in order to investigate the weldability of stainless steels. The evolution of temperature and fluid flow during gas tungsten arc (GTA) welding is investigated. The physical model takes into account heat and mass transfer, electric transport and resulting magnetic field, it considers Marangoni force, self-induced electromagnetic force and buoyancy force for the weld pool convection. This model has been implemented in Code_Saturne® (CFD open source code developed by EDF R&D) and used to compute the numerical results presented in the present paper. These numerical results are validated by experiments carried out using different welding parameters and two 304L stainless steel sulfur concentrations.*

Keywords: Welding, Marangoni effects, Stainless steel

1 Introduction

Because of its high quality of weld metal and weld bead surface, GTA welding is one of the most used arc welding processes. However, weld pool convection and the resulting thermal kinetic can affect the microstructure and material properties of the resultant weld. Convection in the weld pool and consequently the shape of the weldment depends on the balance among several forces, which includes Marangoni force, electromagnetic force and buoyancy force. The Marangoni force, which depends on surface tension gradient, can be the main factor involved in weld pool convection. Heiple et al. [1] showed that trace elements alter fluid flow patterns by changing surface tension gradients on the weld pool surface.

Recently, some authors studied fully coupled arc/weld pool models to deal with the whole problem [2,3]. Brochard [2] proposed a 2D axisymmetric steady-state model. However, only spot welding configuration is considered. The main weakness of the weld pool model proposed by Hamide [4] is that the surface tension gradient is fixed to an arbitrary constant value, and thus the computed weld shapes are dependent on the chosen value. In the hybrid 2D-3D model of Tradia [3], one level of stainless steel sulfur concentration (0.003 wt %) is considered and a constant value of the surface tension gradient is used.

In the present paper numerical and experimental investigations of surface tension effects on weld pool shape are reported for two configurations of GTA welding: spot welding (with fixed energy source) and standard welding without supplying filler metal. In order to validate the numerical model, experiments are carried out using different welding parameters, considering two levels of 304L stainless steel sulfur concentration and taking into account the dependence of surface tension gradient on temperature and sulfur content. During the experiments, thermal time evolutions were measured at different positions using thermocouples and surface evolutions of weld pool were visualized using high speed camera. Weld bead sizes were obtained from macrographs done after polishing and etching weld cross-section. The computed

results are compared with the corresponding experimental ones for specimens containing low sulfur (0.007 wt %) and high sulfur (0.028 wt %), respectively.

2 Computational model

The set of governing equations includes both the Navier-Stokes equations in the melt and Maxwell's electromagnetic equations. *Code_Saturne*® software is used to implement the developed model. In the developed numerical model, it has been assumed that the liquid metal flow is incompressible, Newtonian and laminar; the heat and current source from the arc torch have Gaussian distribution; the weld pool surface remains horizontal and flat and the liquid fraction varies linearly with temperature in the solidification range. Energy loss is taken into account through constant emissivity and heat transfer coefficient.

2.1 Governing equations

Based on the above assumptions, the governing equations can be expressed as follows:

$$\text{- Conservation of mass:} \quad \frac{\partial \rho}{\partial t} + \text{div}(\rho \mathbf{u}) = 0 \quad (1)$$

where ρ is the density and \mathbf{u} the velocity fields.

$$\text{- Conservation of momentum:} \quad \frac{\partial}{\partial t}(\rho \mathbf{u}) + \text{div}(\rho \mathbf{u} \otimes \mathbf{u}) = \text{div}(\boldsymbol{\sigma}) + \rho \mathbf{g} + \mathbf{j} \times \mathbf{B} + \mathbf{S}^u \quad (2)$$

where $\boldsymbol{\sigma}$ is the stress tensor given by equation (3a), \mathbf{g} the gravity acceleration, \mathbf{j} the current density, \mathbf{B} the magnetic field and \mathbf{S}^u the source term introduced for extinction of the velocity in the solid phase given by equation (4).

$$\boldsymbol{\sigma} = \boldsymbol{\tau} - p \mathbf{Id}, \quad \boldsymbol{\tau} = 2\mu \mathbf{D} - \frac{2}{3} \text{tr}(\mathbf{D}) \mathbf{Id}, \quad \mathbf{D} = \frac{1}{2} (\text{grad } \mathbf{u} + \text{grad } \mathbf{u}^t) \quad (3a-c)$$

where $\boldsymbol{\tau}$ is the shear stress, p the pressure, μ the dynamic viscosity, \mathbf{Id} the identity tensor and \mathbf{D} the strain rate tensor.

The term $\mathbf{j} \times \mathbf{B}$ in equation (2) is the Lorentz force resulting from the electric current present in GTA welding processes. \mathbf{S}^u represents the frictional dissipation in the mushy zone according to Carman-Kozeny equation for flow through a porous media. Brent et al [5] proposed the following expression for this source term:

$$\mathbf{S}^u = -C \frac{(1-f_l)^2}{f_l^3} \mathbf{u} \quad (4)$$

where C is a constant ($C \approx 10^{18}$) accounting for the mushy region morphology. The liquid fraction f_l is assumed to vary linearly with temperature.

- **Conservation of energy:** By splitting the total enthalpy into the sensible and latent heat contributions, the thermal energy transport in the workpiece can be expressed by the following equation:

$$\frac{\partial}{\partial t}(\rho h) + \text{div}(\rho \mathbf{u} \otimes h) = \text{div} \left(\frac{\lambda}{C_p^{eq}} \text{grad } h \right) + \mathbf{j} \cdot \mathbf{E} \quad (5)$$

where λ is the thermal conductivity and C_p^{eq} the equivalent specific heat according to [6].

The term $\mathbf{j} \cdot \mathbf{E}$ is the volumetric heat source from the Joule effect.

- **Conservation of electrical charge:** The determination of the electromagnetic forces and the joule effect in the computational domain requires the computation of the current density \mathbf{j} , the electric field \mathbf{E} and the magnetic flux \mathbf{B} . To achieve this, the coupled current continuity and the magnetic potential equations are computed as function of the electric potential P_R and the magnetic potential vector \mathbf{A} . Electrical potential is calculated by solving the equation for current continuity:

$$\text{div}(\sigma_e \text{grad } P_R) = 0 \quad (6)$$

where σ_e is the electrical conductivity. The current density is calculated from Ohm's law :

$$\mathbf{j} = -\sigma_e \text{grad } P_R \quad (7)$$

while the potential vector \mathbf{A} is derived from :

$$\text{div}(\text{grad } \mathbf{A}) = -\mu_0 \mathbf{j} \quad (8)$$

where μ_0 magnetic permeability of vacuum.

The electric field \mathbf{E} and the magnetic flux \mathbf{B} are then computed from P_R and \mathbf{A} as follows:

$$\mathbf{E} = -\text{grad}P_R, \mathbf{B} = \text{rot}\mathbf{A} \quad (9)$$

2.2 Boundary conditions

At the top surface, a mixed boundary condition is prescribed as in [13]:

$$\mu \frac{\partial u}{\partial z} = \frac{\partial \gamma}{\partial T} \frac{\partial T}{\partial x}, \mu \frac{\partial v}{\partial z} = \frac{\partial \gamma}{\partial T} \frac{\partial T}{\partial y}, w = 0 \quad (10)$$

where u , v and w are the velocity components along the x , y and z directions, respectively and $\partial\gamma/\partial T$ the temperature coefficient of surface tension. In this study, the thermal surface tension coefficient $\partial\gamma/\partial T$ depends on both temperature and sulfur activity according to Sahoo et al. [7]:

$$\frac{\partial \gamma}{\partial T} = -A - R\Gamma_s \ln(1 + Ka_s) - \frac{Ka_s}{1 + Ka_s} \times \frac{\Gamma_s \Delta H^0}{T} \quad \text{where } K = k_1 \exp\left(-\frac{\Delta H^0}{RT}\right) \quad (11a-b)$$

Where A is a constant negative of $\partial\gamma/\partial T$ for pure metal, a_s is the activity of sulfur, ΔH^0 is the standard enthalpy of adsorption, Γ_s is the surface excess at saturation, k_1 is entropy factor and R is gas constant.

The heat flux φ_{source} and the current density j_z boundary conditions accounting for the energy source at the top surface are defined by the following Gaussian distributions:

$$\varphi_{source}(x, y) = \frac{IU\eta}{2\pi r_t^2} \exp\left(-\frac{x^2 + y^2}{2r_t^2}\right), j_z(x, y) = \frac{I}{2\pi r_e^2} \exp\left(-\frac{x^2 + y^2}{2r_e^2}\right) \quad (5a-b)$$

where I is the electric current, U the voltage, η the arc efficiency, r_t and r_e the heat and current distribution parameters, respectively.

The heat loss by radiation φ_{rad} and convection φ_{conv} respectively through the top, bottom and outer surfaces are defined by the following equations:

$$\varphi_{rad} = \sigma_B \varepsilon (T^4 - T_0^4), \varphi_{conv} = h_C (T - T_0) \quad (13a-b)$$

where σ_B is the Stefan-Boltzmann constant, ε is the emissivity of the body surface, T_0 is the ambient temperature, and h_C is convective heat transfer coefficient.

2.3 Stainless steel thermophysical properties

Table 1 The compositions of the as-received materials

Materials	C	Si	P	S	Cr	Mn	Ni	N	Co
M1	0.020	0.290	0.034	0.026	18.08	1.720	8.020	0.072	0.110
M2	0.025	0.391	0.028	0.007	18.175	1.424	8.054	0.075	0.140

Table 2 Thermo-physical properties for 304L stainless [15].

Properties	Solid phase	Liquid phase
$\rho(kg.m^{-3})$	$A + B \times T + C \times T^2$ $A = 7984.1, B = -2.6506 \times 10^{-1}, C = -1.158 \times 10^{-4}$	$A + B \times T + C \times T^2$ $A = 7551.2, B = -1.1167 \times 10^{-1}, C = -1.5063 \times 10^{-4}$
$C_p(J.kg^{-1}.K^{-1})$	$A + B \times T, A = 4.69 \times 10^2, B = 1.34596$	794.2
$\lambda(W.m^{-1}.K^{-1})$	$A + B \times T, A = 8.116, B = 1.618 \times 10^{-2}$	$A = 12.29, B = 3.248 \times 10^{-2}$
$\mu(kg.m^{-1}.s^{-1})$		$10^{\left(\frac{A}{T} - B\right)}, A = 2.3852, B = 5.958 \times 10^{-4}$

In this study, samples were made of 304L stainless steel with different level of sulfur concentrations, low (0.007 wt%) and high (0.026 wt%) sulfur contents. The nominal compositions of as received 304L stainless steels are given in Table 1. The thermo-physical properties of the 304L stainless steel workpiece listed in Table 2 are taken from [8].

2.4 Analysis of sulfur content effect

The effect of sulfur in GTA welding is studied using the model developed in this study. A Gaussian heat source is applied on the upper surface with $I = 200A$, $U = 12V$, $\eta = 0.7$, $r_t = 5mm$, $r_e = 5mm$, appearing in equations (12a), together with a convective heat transfer coefficient $h_c = 15Wm^{-2}K^{-1}$ and $\varepsilon = 0.5$ appearing in equations (13). The spot welding configuration has been computed using a computational domain modeled with a 3D wedge of 28° containing 750 000 elements while a computational domain of 2 000 000 elements is used in the case of standard welding.

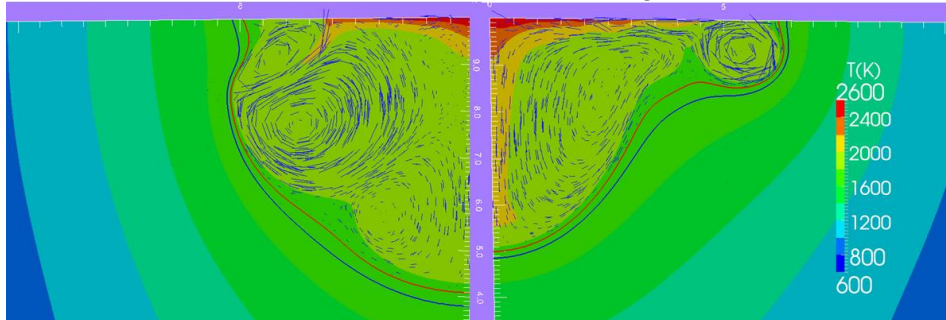


Fig 1 Computed flow pattern in the molten pool for 0.026 wt% (at left) and 0.007 wt% (at right) of sulfur content in spot welding configuration

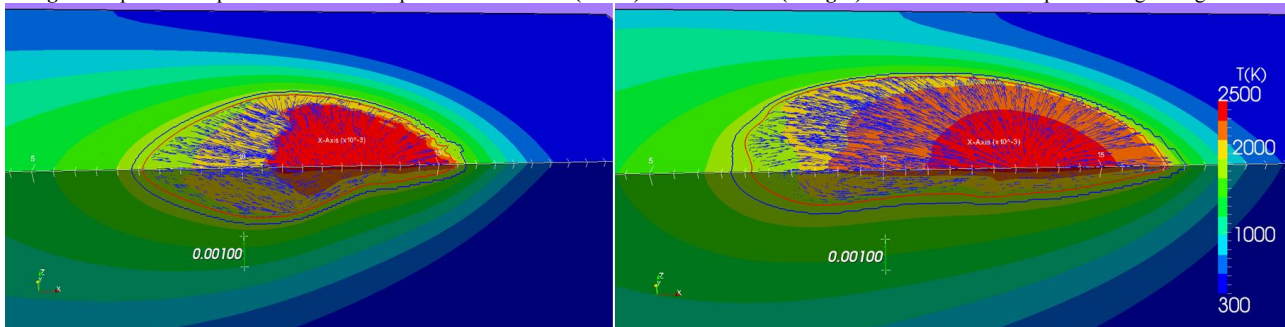


Fig 2 Computed flow pattern in the molten pool for 0.026 wt% (at left) and 0.007 wt% (at right) of sulfur content in standard welding configuration

It can be observed from Fig 1 and Fig 2 that a radically different fluid flow structure takes place in the case of high sulfur content (0.026 wt%) compared to the case of low sulfur content (0.007 wt%). It can also be seen from these figures that the weld pool is deeper in the case of 0.026 wt% sulfur content than the 0.007 wt% one while its width is more important for the 0.007 wt%. These results corroborate the well known effect of sulfur on the weld pool.

3 Experimental procedure

The experimental setup is constituted by the welding process including welding generator and torch, the welding robot, thermocouples, high speed camera, and a personal computer for control and acquisition. During the process, thermal time evolutions were recorded at several locations of the workpiece surface using K type thermocouples of 0.5 mm diameter at 20 Hz sampling frequency. To prevent the weld from atmospheric contamination and oxidation, a pur argon gas was supplied at a flow rate of 15 l/mn. A thoriated tungsten electrode (W-2 % ThO₂) was used in the experiments and its vertex angle was 40°.

A high speed video camera with 1000 Hz framing rate was used to observe the GTA weld pool surface in the real time and a 20 W laser diode provided a synchronized lighting. The welding scene was filtered with a 808 nm width band pass filter to attenuate arc light for clear images of weld pool growth (Fig 3a). So, time evolution of weld pool radius can be measured. After welding, the weld pool geometry was revealed thanks to post mortem macrography and enabling to measure weld pool width and penetration using conventional polishing and etching techniques (Fig 3b).

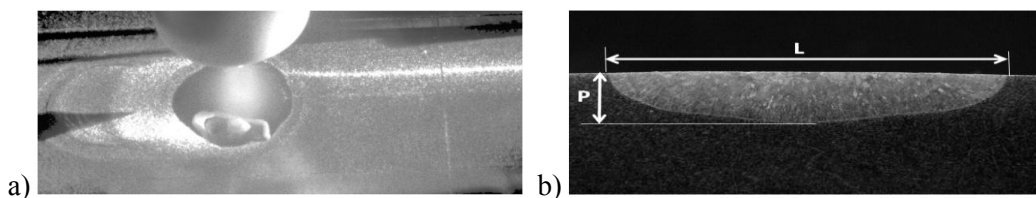


Fig 3 a) Image from high speed camera shows weld pool, b) Example of experimental macrography shows the weld pool sizes.

Experiments were performed using 200 A direct current and 3 mm arc length. Two experimental configurations were considered: First, GTA welding tests were performed with fixed energy source (« spot» welding) on 304L stainless steel sample disks of 100 mm diameter and 20 mm thickness. The welding power was kept long enough (20 s) at samples' center to ensure a fully developed weld pool. Thermal time evolution was recorded with 3 thermocouples (T1, T2, T3) positioned at 11.5, 13.5, and 16 mm (respectively) from the center of the weld pool. In a second experimental configuration, GTA bead-on-plates were carried out without supplying filler metal on plates 70 mm width, 70 mm length and 20 mm thickness. For these experiments, two values were used for the welding velocity (15 cm/min and 30 cm/min).

4 Results and discussions

- Analysis of energy source characteristics

The thermal time evolutions are used to validate energy source characteristics used for calculations in the present study. For doing this, the calculated thermal time evolutions at three positions on the sample are compared to measured ones. A fairly good agreement is obtain as shown in Fig 9, but it can be seen that the measured temperatures decrease slightly faster than the calculated ones. The closer to the energy source, the higher are the discrepancies between experimental and computational solutions.

This difference can be attributed to either an improper value of the global process efficiency coefficient η or the heat losses by radiation and convection. In the computations, η is set to 0.8 and constant values were used for h_c and ε . But in reality, η can be slightly different from this value and the heat loss parameters vary from the center of the weld pool to the end of the specimen due to the high temperature difference.

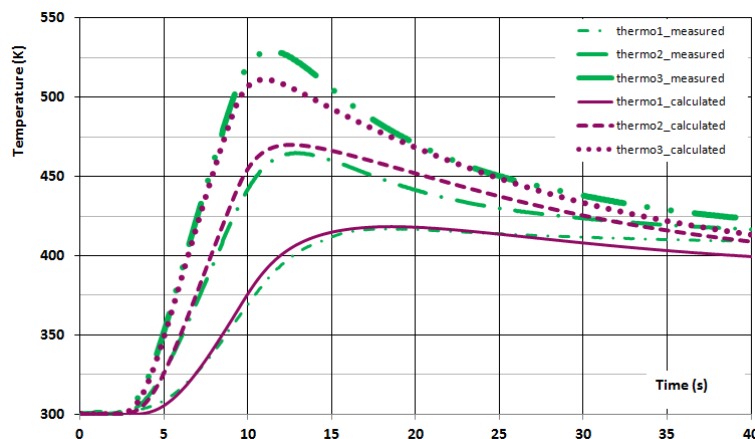
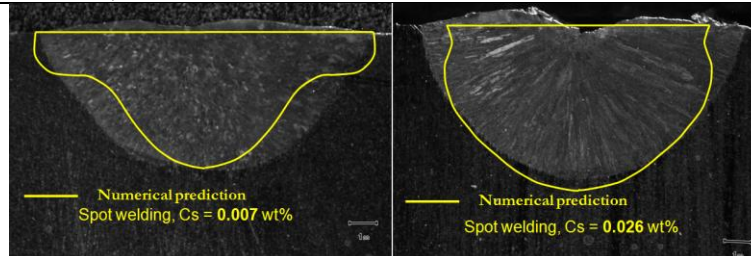
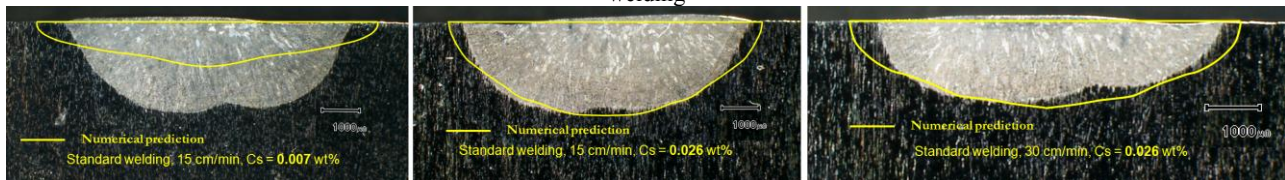


Fig 4 Experimental and calculated temperature evolutions for GTA spot welding (thermocouples positions from the center of the weld pool: thermo1 at 11.5 mm, thermo2 at 13.5 mm and thermo3 at 16 mm).

Table 3 shows the comparison of experimental and computed weld pool sizes. It can be seen from Fig 5 and Fig 6 that for different welding configurations the weld pool shape is better reproduced by the computation in the case of high sulfur content than in the case of lower sulfur content. This can be attributed to either the presence of other alloying elements or the model of surface tension used. In the present study, only the effect of sulfur content is considered and the surface tension of the metal is modeled as for binary metal. The activities of manganese in the liquid metal from high sulfur steel would be lower than that in the low sulfur steel. This is because in the low sulfur steel, very little MnS precipitates is present. In contrast, the manganese is mainly present as MnS in the high sulfur steel. As result, during welding, the vaporization of Manganese in the liquid metal from low sulfur content is high than in the high sulfur content. This would lead to high variation of the alloying elements contents in the low sulfur content and consequently the sulfur activity should be more important than in the original metal.

Table 3 Welding variables and experimentally measured weld pool penetration and width

Welding configuration, Material sulfur content	Weld pool depth (mm)		Weld pool width /2 (mm)	
	Experimental	Calculated	Experimental	Calculated
Spot welding, Cs = 0.007 wt%	5.1 ±0.1	5.1	6.1 ±0.2	6.3
Spot welding, Cs = 0.026 wt%	5.6 ±0.1	6.1	5.9 ±0.2	5.1
Standard welding, 15 cm/mn, Cs = 0.007 wt%	2.2 ±0.1	1.1	3.9 ±0.2	4.8
Standard welding, 15 cm/mn, Cs = 0.026 wt%	2.4 ±0.1	2.5	3.9 ±0.2	4.3
Standard welding, 30 cm/mn, Cs = 0.026 wt%	1.5 ±0.1	1.5	3.3 ±0.2	3.6

**Fig 5** Experimental and calculated weld pool shapes for spot welding**Fig 6** Experimental and calculated weld pool shapes for standard welding

5 Conclusions

In order to investigate the weldability of stainless steels, the effect of surface-active elements especially sulfur on weld pool shape has been studied through a numerical model for GTA welding developed in *Code Saturne*®. Numerical results computed using the presented model have been compared with the corresponding experiments. It has been shown that the model is more representative in the case of high sulfur content than in the case of low sulfur content. On the other hand, for industrial applications it is also an important issue to address the assembly of stainless steel plates of different material compositions and more especially sulfur content. Therefore, work is in progress in this direction for the numerical modeling perspective.

References

- [1] Heiple, C. R., Roper, J.R. 1982. Mechanism for minor element effect on GTA fusion zone geometry. Supplement o the Welding Journal. pp. 97s – 102s.
- [2] Brochard, M. Modèle couplé cathode-plasma-pièce en vue de la simulation du procédé de soudage à l'arc TIG. Université de Provence (Aix-Marseille I). Thèse de doctorat 2009.
- [3] Traidia, A. Multiphysics modelling and numerical simulation of GTA weld pools. Ecole Polytechnique, ENSTA, Palaiseau, PhD Thesis 2011.
- [4] Hamide, M. Modélisation numérique du soudage à l'arc des aciers. Ecole Nationale Supérieure des Mines de Paris. Thèse de doctorat 2008.
- [5] Brent, A.D., Voller, V.R., Reid, K.J. 1988. Enthalpy-porosity technique for modeling convection – diffusion phase change: application to the melting of a pure metal. Numerical Heat Transfer. Vol. 13. pp. 297 - 318
- [6] Comini, G. S., Del Guicide, Saro, O. 1989. Conservative equivalent heat capacity methods for nonlinear heat conduction. Proceedings of the 6th Int. Conf. of Num. Meth. in Thermal Problems. Vol. 6. Part I. pp: 5 - 15
- [7] Sahoo, P., Debroy, T., McNallan, M. 1998. Surface tension of binary metal - surface active solute systems under conditions relevant to welding metallurgy. Metallurgical and Materials Transactions. 19. Vol.B.
- [8] Kim, C.S., 1975. Thermophysical properties of stainless steels. Base Technology.